Review

Influence of Reduction Promoters on Stability of Cobalt/γ-Alumina Fischer-Tropsch Synthesis Catalysts

Gary Jacobs, Wenping Ma and Burtron H. Davis *

Center for Applied Energy Research, 2540 Research Park Drive, Lexington, KY 40511, USA;
E-Mails: gary.jacobs@uky.edu (G.J.); wenping.ma@uky.edu (W.M.)

* Author to whom correspondence should be addressed; E-Mail: burtron.davis@uky.edu;
Tel.: +1-859-257-0251; Fax: +1-859-257-0302.

Abstract: This focused review article underscores how metal reduction promoters can impact deactivation phenomena associated with cobalt Fischer-Tropsch synthesis catalysts. Promoters can exacerbate sintering if the additional cobalt metal clusters, formed as a result of the promoting effect, are in close proximity at the nanoscale to other cobalt particles on the surface. Recent efforts have shown that when promoters are used to facilitate the reduction of small crystallites with the aim of increasing surface Co^0 site densities (e.g., in research catalysts), ultra-small crystallites (e.g., <2–4.4 nm) formed are more susceptible to oxidation at high conversion relative to larger ones. The choice of promoter is important, as certain metals (e.g., Au) that promote cobalt oxide reduction can separate from cobalt during oxidation-reduction (regeneration) cycles. Finally, some elements have been identified to promote reduction but either poison the surface of Co^0 (e.g., Cu), or produce excessive light gas selectivity (e.g., Cu and Pd, or Au at high loading). Computational studies indicate that certain promoters may inhibit polymeric C formation by hindering C-C coupling.

Keywords: Fischer-Tropsch synthesis; cobalt; deactivation; promoters

1. Introduction

Fischer-Tropsch synthesis (FTS) making use of cobalt catalysts is the core of the gas-to-liquids (GTL) process [1,2]. Due to the high H_2/CO syngas ratio derived from reforming of natural gas,

additional water gas shift is not required to adjust the ratio upward, and internal water-gas shift (WGS) activity is undesirable. This is one benefit of cobalt catalysts relative to iron catalysts for GTL, as the former typically possess low intrinsic WGS activity. Because cobalt is much more expensive than its iron counterpart, and because the reaction occurs on the surface, it is important to disperse the cobalt metal particles in order to improve usage efficiency.

A typical cost effective way to do so is to impregnate the pre-calcined support with a cobalt nitrate solution by wet or dry (incipient wetness) impregnation followed by drying, air calcination to decompose the cobalt nitrate precursor to cobalt oxide, and reduction (e.g., 10 h in hydrogen gas at 350 °C) to Co^0 crystallites (typically in the range of 5 to 20 nm). The surface of Co particles provides the catalytically active sites for Fischer-Tropsch synthesis.

However, with typical reduction of supported cobalt at low temperatures (e.g., 350–400 °C) appropriate for obtaining active small crystallites of 6–15 nm, a sizeable fraction (typically in the range of 15–70%) of the cobalt remains in the oxide form, mainly as CoO. The fraction of unreduced cobalt is larger for supports such as alumina which interact strongly with cobalt oxide and for low cobalt loadings, e.g., less than 10–15% on such supports. The extent of the interaction increases with decreasing loading of cobalt. At low loadings (e.g., < 5%), 60 to 80% of the cobalt is present as CoO strongly bound to the support surface, *i.e.*, a surface cobalt aluminate, $CoO*Al_2O_3$, which requires very high temperatures to reduce [3]. At high loadings (e.g., 15%–30%Co), cobalt will be present primarily as Co_3O_4, which reduces in two steps: $Co_3O_4 + H_2 = 3CoO + H_2O$ and $3CoO + 3CoO = Co + 3H_2O$, for which maximum rates of reduction occur at about 300–350 and 500–650 °C, respectively [4]. Thus, following reduction of an unpromoted 15–30% Co/alumina at 350–400 °C for 5–15 h, a significant fraction (30–60%) of CoO typically remains [5–8]. Since higher extents of reduction (80–90%) of cobalt are highly desirable, *i.e.*, correlated with higher activity on a per g catalyst basis, as well as improved C_5+ selectivity, there is considerable interest and widespread application of noble metal promoters, which facilitate the reduction of cobalt oxides and increase the surface density of cobalt active sites.

This article reviews a number of stability issues associated with the application of promoters for cobalt FTS catalysts. Examples are provided to demonstrate a number of considerations for selecting a noble metal for Co catalysts. The main point of the article is that each promoter has its own advantages and set of issues that must be addressed and, in some cases, still defined.

2. Results and Discussion

Figure 1 compares temperature programmed reduction (TPR) TPR profiles of a number of noble metal and Group IB-promoted 15%Co/γ-Al$_2$O$_3$ catalysts pertinent to this review. The commonly used promoters are Pt, Re, and Ru and the solid line profiles are at close to atomically equivalent loadings. Pt and Ru facilitate the reduction of both steps of cobalt oxide reduction, while Re catalyzes the reduction of primarily the second step. This has been explained by Re oxide reducing at a higher temperature than Pt and Ru and that a reduced form of the promoter is required to obtain the promoting effect [7]; however, further confirmation of this is needed as the oxidation state remains in question [9]. Both Pt and Re appear to be more effective at facilitating reduction relative to Ru, but higher loadings of Ru can be used to further facilitate reduction, as indicated by the dashed profile at 0.5%Ru loading.

Similar trends were reported in the TPR peak locations in a recent investigation of promoter characteristics by Cook *et al.* [9], as shown in Figure 2.

Figure 1. TPR profiles demonstrate the effectiveness of Cu for facilitating reduction of cobalt oxides. Curve labels: unpromoted 15%Co/Al$_2$O$_3$ (thick solid) and Cu-promoted with 0.033%Cu (thick dashed), 0.49%Cu (thin solid), and 1.63%Cu (thin dash-dotted) by weight. (Reproduced with permission from [7] and [10] Copyright 2002, 2009, Elsevier).
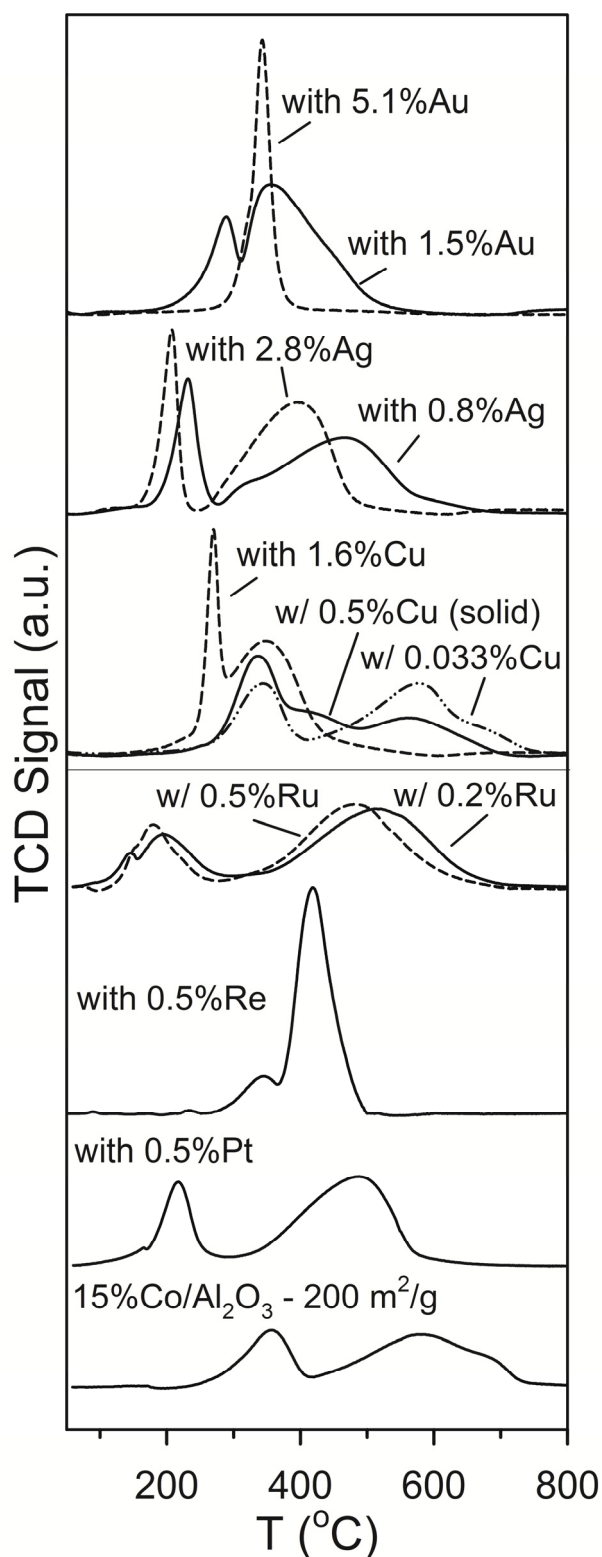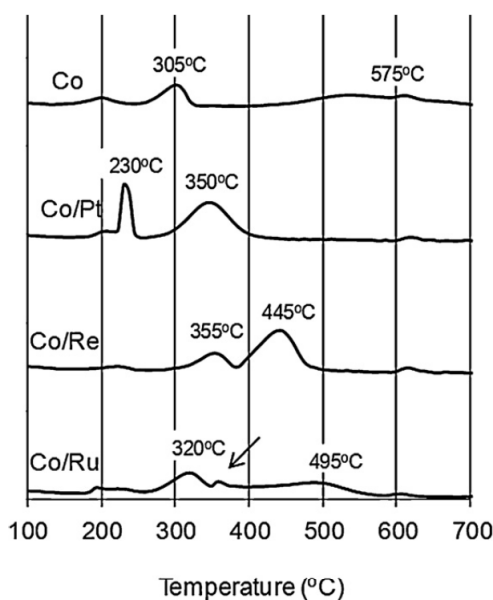
Figure 2. TPR profiles by Cook *et al.* [9] show that Pt and Re are more efficient than Ru in facilitating reduction of cobalt oxides over 25%Co/γ-Al₂O₃ catalysts with equivalent atomic loading (*i.e.*, noble metal / Co ratio was 0.007).

Cu, Ag, and Au (Group IB) promoters are also effective at promoting the reduction of cobalt oxides, as described in Figure 1 (top) [10]. However, note that the loadings indicated by the solid lines are approximately three times higher on an atomic basis than those of the commonly used promoters (Pt, Re, Ru) shown in the lower part of the figure. The costs of Ag and Cu are, whether on a weight or atomic basis, much lower than any of the other promoters shown. Therefore, it was of interest to explore their ability to facilitate reduction at even higher loadings. Increasing the loading by a factor of 3.3 resulted in further and important shifts of both TPR peaks of cobalt oxide reduction to lower temperatures (Figure 1, top).

The choice of promoter metal and its loading may influence the stability of cobalt catalysts in a number of ways. The first section examines how reduction promoter type and loading influence the activity and selectivity of cobalt catalysts, while the second section discusses how promoters may exacerbate deactivation rates through oxidation and a possible complex sintering mechanism, the two of which are not mutually exclusive. A brief summary of the application of computational methods is also provided, which discusses the location of promoter relative to cobalt, the resistance or sensitivity of cobalt to oxidation depending on size, and how promoters may hinder carbon formation pathways. Finally, in adding a second catalytic metal to the catalyst, the ability to regenerate the catalyst in a simple and effective manner becomes an important concern.

2.1. Influence of Promoter Choice and Loading on Catalyst Activity and Selectivity

2.1.1. Example #1—Copper

The first example demonstrates a relatively inexpensive metal that is highly effective for promoting the reduction of cobalt oxides: Cu, which is a common promoter in iron carbide FTS catalysts [11,12].

As of this writing, Cu is approximately 0.015% of the cost of Pt on a mass basis and would seem to be an ideal candidate as a promoter.

With increases in extent of reduction of cobalt (from 49.8% for 15%Co/Al_2O_3 to 53.2, 69.4, and 93.3% for 0.033%, 0.49%, and 1.63% Cu-promoted 15%Co/Al_2O_3 catalysts, respectively) the active metal site densities with Cu addition increased also, and hydrogen chemisorption uptakes measured by TPD increased from 72 µmol H_2/g_{cat} for the unpromoted 15%Co/Al_2O_3 catalyst to 82, 140, and 172 µm H_2/g_{cat} for the 0.033%, 0.49%, and 1.63% Cu-promoted 15%Co/Al_2O_3 catalysts [10]. However, the metal dispersions do not account for the partitioning of metal type on the surface of Co particles, or the influence of the presence of Cu on the ensembles of Co required for conducting the synthesis. Surface enrichment by Cu has been detected in bimetallic Cu-Co catalysts before [13].

Table 1 shows a comparison of X_{CO} at the same weight hourly space velocity of two Cu-promoted 15%Co/Al_2O_3 catalysts relative to the unpromoted 15%Co/Al_2O_3 catalyst. Despite increases in metal site densities as measured by hydrogen TPD, a decrease in X_{CO} is observed, which is exacerbated at higher Cu loading [10]. These results suggest a poisoning of surface Co sites, likely due to enrichment of Cu at the surface. This finding is further supported by the changes in selectivity that occur when comparing the catalysts to the unpromoted catalyst at a similar conversion level. Table 2 shows that at the lower Cu promoter loading, the methane is slightly increased, C_5+ is slightly decreased [10]. However, increasing the Cu promoter loading further leads to a prohibitive increase in methane selectivity (21.6% *versus* 9.2%) and a precipitous drop in C_5+ selectivity (47.7% *versus* 81.6%) [10].

Table 1. X_{CO} for two Cu promoted 15%Co/Al_2O_3 catalysts at a SV of 4.2 NL/g_{cat}/h relative to the unpromoted catalyst. Conditions: 220 °C, 1.6 MPa, H_2/CO = 2.0 (adapted with permission from [10] Copyright 2009, Elsevier).

Catalyst	TOS (h)	X_{CO} (%)	SV (NL/g_{cat}/h)
15%Co/Al_2O_3	26–98	28.7	4.2
0.49%Cu-15%Co/Al_2O_3	30–99	27.9	4.2
1.63%Cu-15%Co/Al_2O_3	25–104	14.2	4.2

Table 2. Two comparisons of product selectivity at similar X_{CO} levels for two Cu promoted 15%Co/Al_2O_3 catalysts relative to the unpromoted catalyst. Conditions: 220 °C, 1.6 MPa, H_2/CO = 2.0 (adapted with permission from [10] Copyright 2009, Elsevier).

Catalyst	X_{CO} (%)	SV (NL/g_{cat}/h)	S(CH_4)	S(C_5+)	S(CO_2)
15%Co/Al_2O_3	47.8	2.0	8.9	80.6	0.82
0.49%Cu-15%Co/Al_2O_3	50.6	1.7	9.9	76.6	0.83
15%Co/Al_2O_3	28.7	4.2	9.2	81.6	0.67
1.63%Cu-15%Co/Al_2O_3*	29.9	1.0	21.6	47.7	1.51

* Due to the low activity of the 1.63%Cu promoted catalyst, a separate comparison was made at lower X_{CO}, as it was not possible to decrease SV further.

2.1.2. Example #2—Silver and Gold

A comparison between Ag and Au shows that, in the case of Ag promoted 15%Co/Al$_2$O$_3$, the catalyst achieves higher activity (Table 3) and C$_5$+ selectivity (Table 4) than the unpromoted catalyst at both high and low loadings of promoter. A 15% Co/Al$_2$O$_3$ catalyst promoted with 1.51% Au also performs better than the unpromoted catalyst with both an increase in productivity and a slight improvement in selectivities [10]. However, at a higher Au loading (5.05%) the catalyst performed poorly with a steep drop in productivity (from X$_{CO}$ of 51.7 at 1.51%Au to an X$_{CO}$ of 14.1 at 5.05%Au at SV = 4.2, Table 3) and adverse impacts on selectivity (C$_5$+ is 60.1% compared to 81.6% for the unpromoted catalyst at X$_{CO}$ of ~28%, Table 4) [10]. Thus, noble metal loading of promoter is important, not only from the standpoint of cost.

In a recent detailed kinetic investigation [14], which was a collaboration between CAER and Texas A&M University in Qatar, modeling results point to the presence of two kinds of sites on the Co FTS catalyst for the production of methane—FTS sites from standard Anderson-Schulz-Flory kinetics and additional sites for methanation. The results of the Au promoted catalyst at the lower loading, and the Ag promoted catalysts at both low and high loadings, suggest that these Group IB promoters assist in either blocking methanation sites or controlling the relative surface fugacity of hydrogen relative to adsorbed CO and intermediates on the surface of the cobalt catalyst.

Table 3. X$_{CO}$ for two Ag and Au-promoted 15%Co/Al$_2$O$_3$ catalysts at a SV of 4.2 NL/g$_{cat}$/h relative to to the unpromoted catalyst. Conditions: 220 °C, 1.6 MPa, H$_2$/CO = 2.0 (adapted with permission from [10] Copyright 2009, Elsevier).

Catalyst	TOS (h)	X$_{CO}$ (%)	SV (NL/g$_{cat}$/h)
15%Co/Al$_2$O$_3$	26–98	28.7	4.2
1.51%Au-15%Co/Al$_2$O$_3$	26–57	51.7	4.2
5.05%Au-15%Co/Al$_2$O$_3$	30–84	14.1	4.2
0.83%Ag-15%Co/Al$_2$O$_3$	20–47	50.4	4.2
2.76%Ag-15%Co/Al$_2$O$_3$	22–92	46.9	4.2

Table 4. Product selectivities for Ag and Au-promoted 15%Co/Al$_2$O$_3$ catalysts at X$_{CO}$ values comparable to the unpromoted catalyst. Conditions: 220 °C, 1.6 MPa, H$_2$/CO = 2.0 (adapted with permission from [10] Copyright 2009, Elsevier).

Catalyst	X$_{CO}$ (%)	SV (NL/g$_{cat}$/h)	S(CH$_4$)	S(C$_5$+)	S(CO$_2$)
15%Co/Al$_2$O$_3$	47.8	2.0	8.9	80.6	0.82
1.51%Au-15%Co/Al$_2$O$_3$	50.0	4.2	8.0	83.7	0.83
0.83%Ag-15%Co/Al$_2$O$_3$	50.4	4.2	7.7	83.6	0.94
2.76%Ag-15%Co/Al$_2$O$_3$	46.9	4.2	7.6	85.0	0.87
15%Co/Al$_2$O$_3$	28.7	4.2	9.2	81.6	0.67
5.05%Au-15%Co/Al$_2$O$_3$*	27.1	1.0	18.0	60.1	1.68

* Due to the low activity of the 5.05%Au promoted catalyst, a separate comparison was made at lower X$_{CO}$, as it was not possible to decrease SV further.

2.1.3. Example #3—Common Promoters (Pt, Re, Ru)

Slight differences in selectivity can also be achieved with the commonly used reduction promoters, which are Pt, Re, and Ru [15], as compiled in Table 5. Ruthenium itself is catalytically active for the FTS reaction, and higher alpha values have been measured in the hydrocarbon distribution [16]. Therefore, it is not surprising that lower methane and higher C_5+ were achieved with a 0.26%Ru-25%Co/Al_2O_3 catalyst relative to an unpromoted one. Re promoter was also found to give slightly better selectivities, in agreement with the work of Borg *et al.* [17] (Table 6). However, an atomically equivalent amount of Pt slightly (though not prohibitively) worsened the selectivities, and an attempt to use Pd to replace Pt resulted in a significantly poorer product distribution.

Table 5. Product selectivities[*] for 25%Co/Al_2O_3 catalysts containing commonly used promoters (Pt, Re, Ru) or Pd at X_{CO} values comparable an unpromoted reference catalyst. Conditions: 220 °C, 2.2 MPa, $H_2/CO = 2.1$ (adapted with permission from [15] Copyright 2012, Elsevier).

Catalyst	X_{CO} (%)	SV (NL/g_{cat}/h)	$S(CH_4)$	$S(C_5+)$
25%Co/Al_2O_3	49.4	4.3	7.9	83.4
0.26%Ru-25%Co/Al_2O_3	51.3	7.6	7.0	86.8
0.48%Re-25%Co/Al_2O_3	49.6	8.0	7.2	86.0
0.50%Pt-25%Co/Al_2O_3	48.0	5.6	8.3	83.0
0.27%Pd-25%Co/Al_2O_3	50.3	4.9	11.5	75.9

[*] $S(CO_2)$ ranged from 0.35–0.75% in all catalysts. All data taken within first 81 h on-stream.

Table 6. Product selectivities from data taken at 210 °C, 2.0 MPa, $H_2/CO = 2$, and X_{CO} of 43–44% (adapted with permission from [17] Copyright 2009, Elsevier) over 20%Co/γ-Al_2O_3 catalysts without or with 0.5%Re using narrow pore (7.4 nm), medium pore (12.3 nm), and wide pore (16.7 nm) supports.

Catalyst	Hydrocarbon selectivity (%)		
	C_1	C_2-C_4	C_5+
Co/NPA	9.0	9.9	81.1
CoRe/NPA	8.8	9.5	81.7
Co/MPA	8.6	8.7	82.8
CoRe/MPA	8.4	8.3	83.4
Co/WPA	8.0	7.5	84.5
CoRe/WPA	8.0	7.2	84.9

In terms of differences in catalyst structure, the three commonly used promoters have, in a number of cases, been observed to be in atomic contact with Co (e.g., as an alloy), with no presence of promoter-promoter coordination at relatively low loadings (Re [18–20], Ru [21], Pt [22–24]). This is not always the case (e.g., Ru [9,16]), indicating that loading and preparation method are also factors that influence coordination environment. Pretreatment is also a factor. For example, Iglesia *et al.* [25] noted with Ru-Co/TiO_2 catalysts that, with increasing calcination temperature, total coordination of Ru

with neighbors increases to suggest sintering, but that most of the increase in coordination is due to Ru taking on coordination with Co; thus, calcination promoted mixing of the two metals.

Moreover, Chonco *et al.* [26] have recently demonstrated with physical mixtures of Pt/Al_2O_3 and Co/Al_2O_3 that atomic coordination of the promoter to cobalt is not always required to obtain a reduction promoting effect. In our work, unlike the Re, Ru, and Pt promoted Co/alumina catalysts at low promoter loadings, Pd promoter exhibited some promoter-promoter (*i.e.*, Pd-Pd) coordination, suggesting the presence of well dispersed islands of Pd that likely gave rise to excessive hydrogenation activity [15] and rapid deactivation relative to the other three promoted catalysts [15].

Considering commercial research, a patent by Sasol researchers [1] examined Ru and Re promoters (of a catalyst containing 30 g Co and 100 g Al_2O_3) at 0.41 g and 3.0 g levels, respectively, *versus* a catalyst containing just 0.05 g of Pt and reported slightly higher productivity with the Pt promoted catalyst (0.349 kg HC/kg cat/h at X_{CO} = 87 vol.% with Pt *versus* 0.307 and 0.281 kg HC/kg cat/h for Ru and Re at X_{CO} = 77 and 70%, respectively). The conditions were 220 °C, 2.0 MPa, H_2/CO = 2/1; space velocity of 2.0 m_n^3/h/kg catalyst. Under the same conditions, similar productivity (~0.29 kg HC/kg cat/h at X_{CO} = 73 vol.%) was observed with a 0.28 g Ru as with 0.05 g Pt with catalysts of lower loading (20 g Co and 100 g Al_2O_3). The results appear to indicate that Pt is a very efficient promoter.

In a patent by Conoco researchers [27], the benefit of adding Re on selectivity was highlighted. Examples 27 through 31 in that patent compare 1%Re promoted 20%Co/Al_2O_3 catalysts with an unpromoted catalyst. Higher conversions (77–100%) and C_5+ productivities (240–270 g/h/kg$_{cat}$) for the Re promoted catalysts relative to the unpromoted catalyst (X_{CO} of 65% and C_5+ productivity of 170 g/h/kg$_{cat}$) were reported. In addition, improvements in selectivities were observed as well, including improvements in alpha (0.89–0.90 with Re promotion *versus* 0.88 for the unpromoted catalyst) and decreases in methane (9–15 wt.% for Re promoted *versus* 18 wt.% for the unpromoted catalyst). Many other examples of Re promotion only or in combination with other elements are also highlighted in the patent report.

2.1.4. Example #4—Impact of Loading for Pt and Ag Promoted Catalysts

The final example is provided to show that, just because the promoter forms promoter-promoter bonds (*i.e.*, as in the case of Pd described in the previous subsection), it should not immediately be ruled out. Ag, by itself, is a catalyst that is only weakly active for hydrogenation, and its addition as a promoter does result in significant Ag-Ag coordination, but the resulting activity and selectivity of the Co catalyst is improved. Figure 3 (left) compares the Ag K-edge EXAFS Fourier transform magnitude spectra of Ag-promoted 25%Co/Al_2O_3 catalysts as a function of Ag loading. While a lower distance peak for Ag-Co coordination is suggested (and confirmed by EXAFS fittings), with increasing loading of Ag, the general trend in EXAFS fittings for Ag-promoted 25%Co/Al_2O_3 catalysts was increasing Ag-Ag coordination (higher distance peak), such that the N_{Ag-Co}/N_{Ag-Ag} ratio decreased from 0.59 at 0.276%Ag loading to 0.16 at 2.76%Ag loading [28].

Figure 3 (right) compares the Pt L_{III}-edge EXAFS Fourier transform magnitude spectra of Pt-promoted 25%Co/Al_2O_3 catalysts. A single low distance peak indicates primarily Pt-Co coordination, with no visible Pt-Pt coordination being evident. As shown in Table 7, as loading was increased for the Pt promoted catalyst, a slight negative impact on selectivity occurred, with a slight

decrease in C_5+ and a slight increase in the WGS rate [28]. For all Pt-promoted catalysts, slightly lower C_5+ selectivities were observed compared to the unpromoted catalyst. With the Ag-promoted catalysts, C_1 and C_5+ selectivities were slightly improved at all loadings [28]. Thus, the presence of a weakly hydrogenating metal [29], Ag, did not adversely affect selectivity to a significant degree, even when excessive amounts of promoter were added [28].

In summary, the above examples show that (1) metals that facilitate reduction of cobalt oxides do not automatically increase X_{CO} on a per gram of catalyst basis; (2) type and loading of promoter influence activity and selectivity such that a metal that may promote X_{CO} (on a per g basis) at lower loading may or may not poison or adversely impact surface fugacities (and selectivity) at higher loadings; and (3) the intrinsic hydrogenation rate of the promoter is an important factor to consider, as it may adversely or beneficially influence selectivity.

2.2. Influence of Promoter Addition on Oxidation and Complex Sintering of Cobalt

2.2.1. Reoxidation of Small Cobalt Crystallites at the Onset of FTS at Realistic Conversions

The primary aims of adding a metal promoters are to (1) lower reduction temperature thereby increasing extent of reduction to Co metal and (2) boost active site densities by facilitating the reduction of cobalt oxide crystallites in strong interaction with the alumina support, such that clusters of cobalt metal crystallites can be formed to provide the active surface for carrying out the FTS reaction. Thus, when a promoter is added, the additional gain in active site density will be due in large part to the reduction of smaller cobalt oxide species having stronger interactions with the support. Depending on the loading of cobalt and method of preparation, if smaller cobalt metal crystallites (e.g., <2–4.4 nm [30,31]) within cobalt clusters are formed, they may be susceptible to reoxidation [30,32]. Some researchers have recently indicated that Co clusters less than 6–8 nm have lower intrinsic activity [33,34]. Additional investigations are needed in this area. At commercially relevant FTS conditions, a problem was identified by us in defining intrinsic activity; as chemisorption is conducted on freshly activated catalysts, any oxidation of such small Co clusters that occurs at commercially relevant conditions can mask a measurement of intrinsic activity at the level of the active site [35]. Therefore, it is important to take into account the oxidation state of Co in the working FTS catalyst.

To probe the role of oxidation, a recent XANES study was made whereby freshly reduced unpromoted and Pt-promoted cobalt/alumina catalysts were subjected to H_2:CO:H_2O mixtures typical of the 50% conversion condition of a slurry phase reactor [36] for one hour. A lower-than-commercial loading of 10% cobalt was utilized in order to favor the formation of small cobalt crystallites after activation that fall in the range of being susceptible to reoxidation. The average cobalt cluster size (*i.e.*, cluster of crystallites) was ~5 nm [36]. Even though the 10%Co/Al_2O_3 catalyst was reduced at 550 °C as opposed to 400 °C for the 0.5%Pt-10%Co/Al_2O_3 catalyst, the extent of reduction from XANES indicated that the Pt-promoted catalyst had a higher extent of reduction, as defined by the intensity of the white line. When switching to conditions to mimic 50% conversion, the white line intensity in the XANES spectra of both catalysts increased significantly (Figure 4), but the change was more severe for the Pt-promoted catalyst [36]. This reoxidation occurred rapidly, is confined to a fraction of cobalt, and is not associated with the initial decay period commonly observed in FTS reaction tests, which

may take on the order of days to establish. Reoxidation of the small cobalt crystallites (<2–4.4 nm) has been recently verified by in-situ XRD and magnetometer investigations [37].

Figure 3. (**left**) Ag promoted 25%Co/Al$_2$O$_3$ catalysts displayed EXAFS peaks that could only be fitted well by including both Ag-Co and Ag-Ag coordination; (**right**) Pt promoted 25%Co/Al$_2$O$_3$ catalysts displayed a single peak in the first coordination shell that could be fitted well by only including Pt-Co coordination (adapted with permission from [28] Copyright 2013, Elsevier).
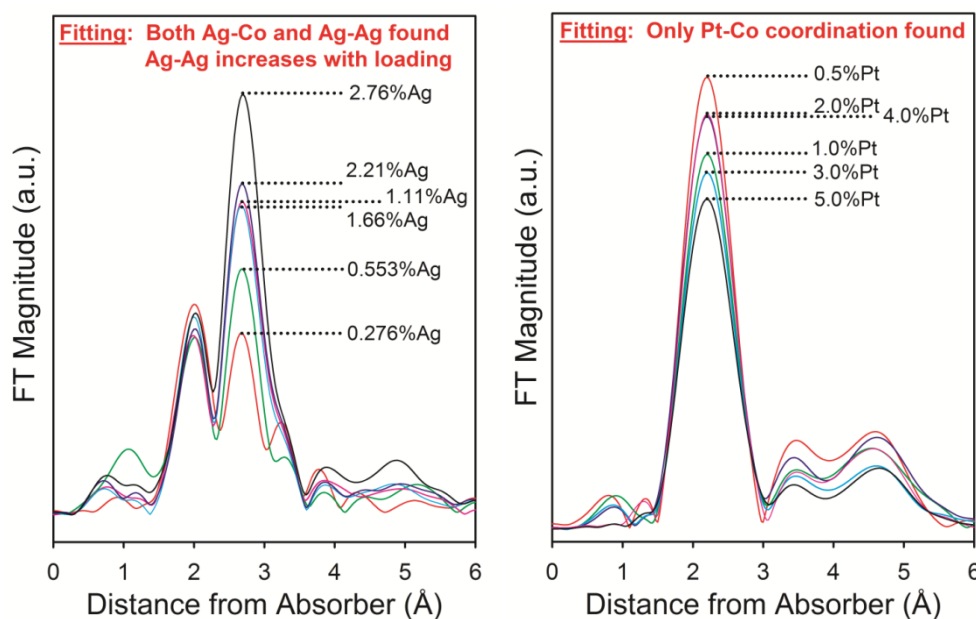

Table 7. Product selectivity * of 25%Co/Al$_2$O$_3$ catalysts having different loadings of Ag and Pt (adapted with permission from [28] Copyright 2013, Elsevier).

Catalyst	X$_{CO}$ (%)	SV (NL/g$_{cat}$/h)	S(CH$_4$)	S(C$_5$+)	S(CO$_2$)
25%Co/Al$_2$O$_3$	51.0	3.4–4.2	8.3	82.5	0.8
0.5%Pt-25%Co/Al$_2$O$_3$	52.0	1.7–12	9.1	81.2	1.1
2.0%Pt-25%Co/Al$_2$O$_3$	45.0	9.0–12	9.1	81.9	1.1
5.0%Pt-25%Co/Al$_2$O$_3$	52.5	10–16	9.5	80.7	3.2
0.276%Ag-25%Co/Al$_2$O$_3$	46.4	8.8–12	7.4	84.1	0.4
1.11 %Ag-25%Co/Al$_2$O$_3$	48.1	9.3–12	7.3	83.7	0.4
2.76%Ag-25%Co/Al$_2$O$_3$	44.5	7.0–12	7.6	84.1	0.6

* All data taken within first 58 h on-stream. *T* = 220 °C; *P* = 2.2 MPa; H$_2$/CO = 2.1.

Figure 4. (**left**) Pt promoted and (**right**) unpromoted 10%Co/Al$_2$O$_3$ catalyst after (solid) hydrogen activation (550 °C for unpromoted and 400 °C for Pt-promoted) and (dashed) after exposure to H$_2$, CO, and H$_2$O partial pressure ratios mimicking X$_{CO}$ = 50% at 20.7 bar (adapted with permission from [36] Copyright 2014, Springer).
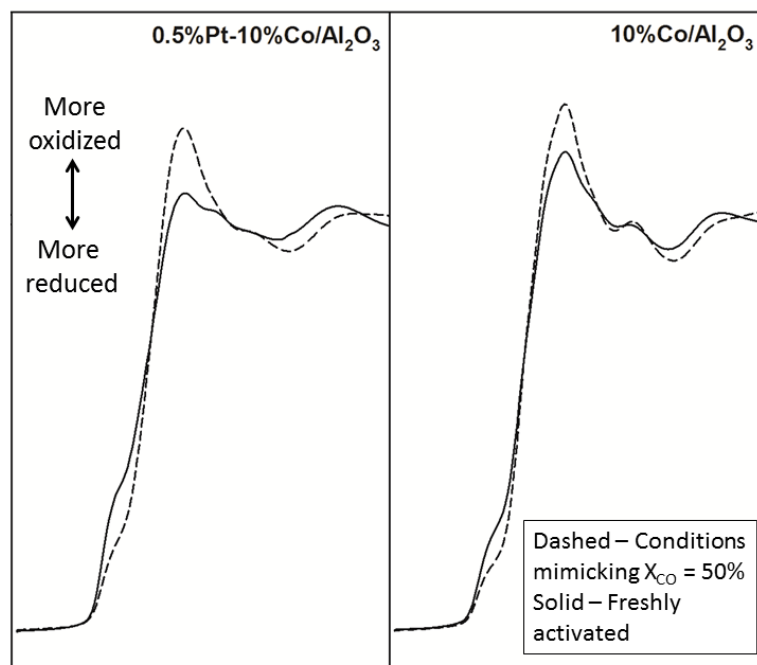
An extreme case in terms of small Co cluster size was also recently examined where Co particles were infused in the pores of KL-zeolite support by a CVD method [35] to produce a 0.5%Pt-5%Co/KL catalyst with 1 nm cobalt particles. The catalyst, following activation in hydrogen, exhibited an extent of reduction of 75%. However, after exposure to FTS conditions (220 °C, 1.8 MPa, H$_2$/CO 1.95, SV of 3.0 NL/g$_{cat}$h), the extent of reduction fell to 33%, as measured by XANES spectroscopy. A loss in Co-Co coordination and growth of Co-O coordination was quantified by EXAFS. X$_{CO}$ fell to 3.0%, and the resulting product selectivities were very poor (CH$_4$ selectivity of 29.6%, C$_5$+ selectivity of 49.8%, and CO$_2$ selectivity of 3.4%).

2.2.2. Sintering and Co Support Compound Formation during Initial Deactivation Period Prior to Leveling-off Period

The mechanisms of sintering during FTS on Co catalysts during typical commercial operation are not well understood and hence will not be discussed in detail in this review. There is evidence to indicate that H$_2$O accelerates sintering of metallic particles [38–41]; on this aspect, a mechanism involving surface oxidation, coalescence, and formation of larger clusters has been postulated by Sadeqzadeh *et al.* [39]. Further research is needed in this area.

Unreduced cobalt oxide in the working FT catalyst could be problematic since it may coalesce, reduce, and provide a driving force for the sintering of cobalt metal particles; this leads to net reduction with time onstream in the initial catalyst decay period (*i.e.*, which follows the onset period of ~1 h as described in the previous section) [32,42]. Moreover, small cobalt oxide species can react with the support and contribute to the formation of cobalt aluminates [42,43]. Since a promoter can

facilitate the reduction of smaller species that may, depending on size, be susceptible to reoxidation at high conversion (as previously described), any cobalt oxide formed at the onset can contribute to either net reduction/sintering with time on-stream or cobalt aluminate formation. Net reduction and changes in Co-Co coordination consistent with sintering were observed for a 0.2%Re-15%Co/Al$_2$O$_3$ research catalyst at CAER during 2000 h of operation (Figure 5) [44,45]. Sintering, *i.e.*, growth of Co metal crystallites, and carbon formation were observed by Saib *et al.* [31] during a 56-day commercial test of a 0.05%Pt/20%Co catalyst. Sintering was determined to be rapid, reaching completion within the initial 15–16 days based on analysis by synchrotron-XRD of samples withdrawn from the reactor during this period; an increase in average crystallite diameter from 9 to 14 nm was observed. Formation in the catalyst of unreactive surface carbons, which restructured or poisoned the catalysts, occurred relatively more slowly over the 56-day period. Carbon deposits were analyzed by TPR during the latter part of this run [46]. During a second 140-day run [32], extent of reduction (EOR) was determined by periodically removing catalyst samples and analyzing them by XANES (Figure 6). EOR was determined to increase from 53 to 89% over the 140-day run. A small amount of cobalt aluminate formation was also observed, as it was detected in a used commercial 20%Co/0.05%Pt/Al$_2$O$_3$ catalyst [31]. Cobalt aluminate was also observed in used 0.2%Re-15%Co/Al$_2$O$_3$ research catalyst samples [44,47] (Figure 7).

Figure 5. (**left**) XANES and (**right**) EXAFS spectra as a function of time for a 0.2%Re-15%Co/Al$_2$O$_3$ catalyst. *T* = 220 °C, 2.0 MPa, SV = 5 SL/h/gcat, H$_2$/CO = 2:1. Adapted with permission from [44] (Copyright 2003, Elsevier) and [45] (2006).
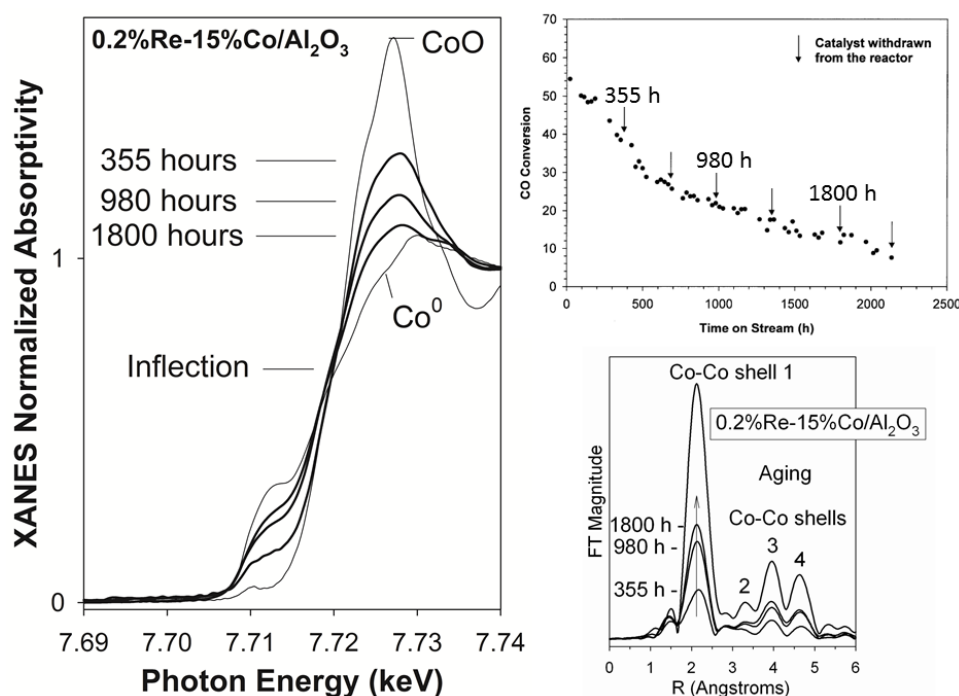
The impact of the promoter on cobalt aluminate formation from initially reduced small Co crystallites is difficult to assess, because unpromoted cobalt/alumina catalysts contain more residual unreduced CoO after activation, and this residual oxide, which is inactive for FTS, can also react with the support to form cobalt aluminate. Thus, there is a question as to how much cobalt aluminate is formed from the oxidation of very small (e.g., <2 – 4.4 nm) crystallites of cobalt metal at the onset of

CoO formation (e.g., within the first hour, as shown in Figure 7 [44,45]) and its subsequent reaction with alumina, and how much is formed from the reaction of residual CoO (*i.e.*, leftover due to incomplete reduction) with the support, as described by Sasol researchers [43]. The cobalt aluminate was detected by them in XANES derivative spectra, as shown in Figure 8. The results from the previous section suggest that the former is dependent on Co crystallite size and $P(H_2O)/P(syngas)$ ratio, which is in turn influenced by conversion level. In a recent kinetic investigation, excursions of a Ru-promoted 25%Co/Al$_2$O$_3$ catalyst (average cluster size of 5.0 nm) to high CO conversion levels (e.g., $X_{CO} > 75\%$) resulted in the oxidation of a fraction of cobalt clusters [21] (as demonstrated by changes in the lineshape of the XANES derivative spectra) and increases in CO_2 and CH_4 selectivities (Figure 9). The oxidized cobalt is active for WGS, and the additional H_2 produced therefrom tends to increase the C_1 product. Thus, there appears to be an unfavorable synergism in the selectivities of CO_2 and C_1 when this threshold is surpassed (Figure 9) [21].

Crystallite size sensitivity for cobalt aluminate formation was also suggested in water co-feeding studies. Although H_2O co-feeding can lead to improvements in activity and selectivity for certain cobalt catalysts [48], when a Pt promoter was utilized to facilitate the reduction of Co oxides in a 15%Co/Al$_2$O$_3$ catalyst (average cluster diameter = 5.6 nm), at 28 vol.% added H_2O the catalyst underwent significant cobalt aluminate formation, as demonstrated in Figure 10 (left) and (right) [49,50] along with catastrophic deactivation (75% drop in X_{CO}). An unpromoted 25%Co/Al$_2$O$_3$ catalyst with larger cluster size (11.8 nm average diameter) [40] was more resistant to this phenomenon. Thus, on the one hand, a promoter is very useful for boosting Co° site densities during activation when the support interaction with Co oxides is high. On the other hand, if the strongly interacting Co oxides are reduced and form tiny Co^0 crystallites on the surface, they are more sensitive to H_2O. Higher loadings can help to make the catalyst more robust by increasing cobalt size, a technique that has been implemented commercially, and thereby reoxidation and subsequent Co aluminate formation may be largely avoided. With a commercial catalyst stabilized against these processes, only up to ~3% cobalt aluminate was formed during realistic FTS conditions [31]. However, it should be noted that when exposed to 1.0 MPa H_2O an increase was observed to 10% cobalt aluminate [43]; thus, water co-feeding or operating at high conversions may have drawbacks, depending on catalyst type and conditions utilized. A schematic of the structural changes discussed for research catalysts, including reoxidation of tiny (<2–4.4 nm) cobalt crystallites at the startup of Fischer-Tropsch synthesis at industrially relevant conversions, is shown in Figure 11 [42].

Figure 6. XANES analysis of a series of used Co/Pt/Al$_2$O$_3$ catalyst samples retrieved from a 100 barrel/day slurry bubble column reactor operated at 220 °C, 2.0 MPa, (H$_2$ + CO) and conversions between 50% and 70%, feed gas composition = 50 vol.% H$_2$ and 25 vol.% CO, P(H$_2$O)/P(H$_2$) = 1–1.5, P(H$_2$O) = 0.4–0.6 MPa. Reproduced with permission from [32]. Copyright (2006) Elsevier.
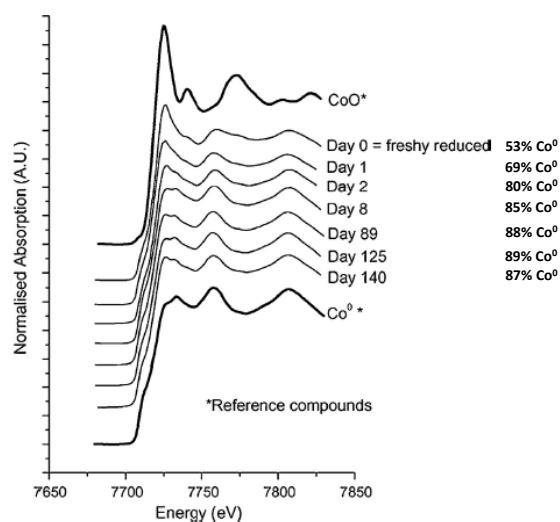

Figure 7. From the run shown in Figure 5, XANES derivative spectra of **(left)** freshly reduced/passivated catalysts, which could be fit with Co^0 and CoO, and **(right)** used catalyst samples, which could only be fitted with Co^0, CoO, and CoAl$_2$O$_4$. Adapted with permission from [44] (Copyright 2003, Elsevier) and [45] (2006).
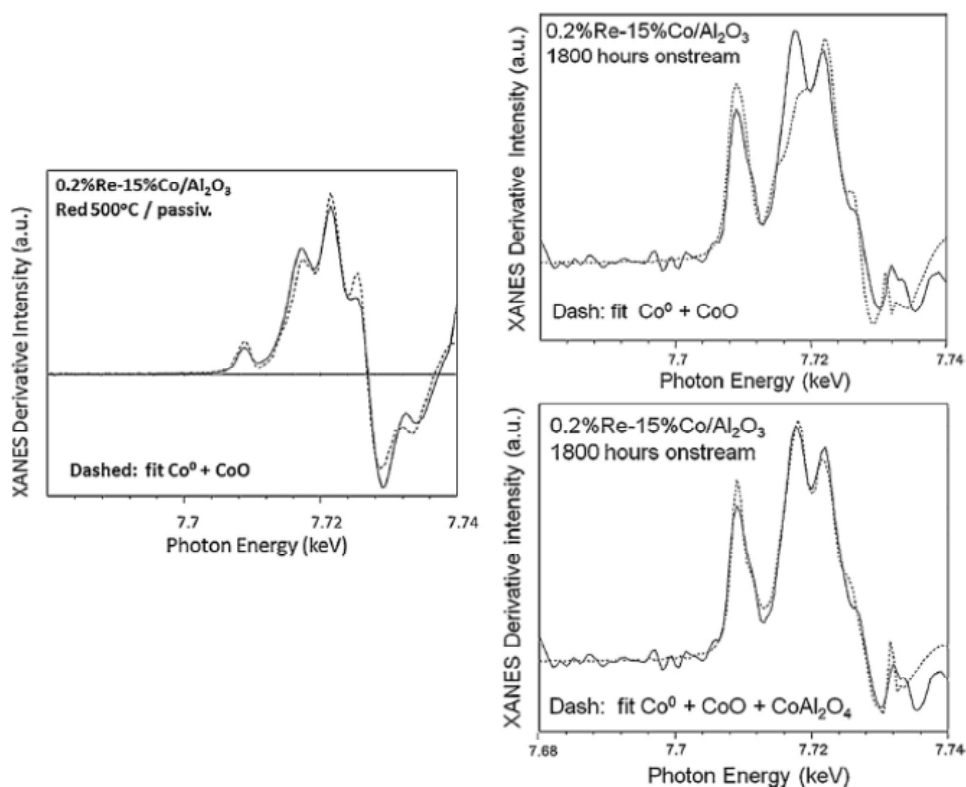
Figure 8. Formation of a minor cobalt aluminate component at 1.0 MPa H_2O by increasing conversion in a continuously stirred tank reactor (CSTR) reactor run at 230 °C, 2.0 MPa, 50 vol.% H_2, 25 vol.% CO and 25 vol.% inerts. Reproduced with permission from [43]. Copyright (2011) Elsevier.
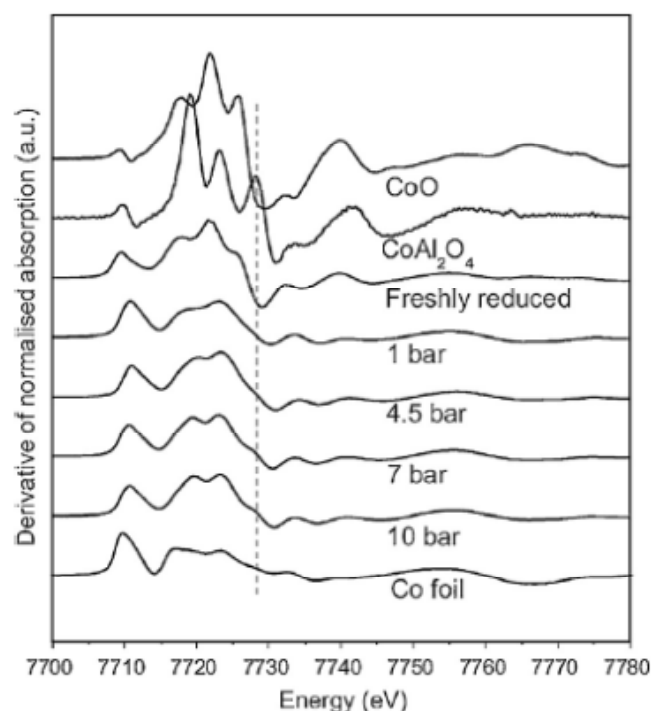

Figure 9. Changes in CO_2 and CH_4 selectivities as a function of conversion over 0.27%Ru-25%Co/Al_2O_3 catalyst (Co cluster size of ~5 nm by hydrogen chemisorption/pulse reoxidation) at 220 °C, 1.5 MPa, H_2/CO = 2.1 and SV = 0.3–15 NL/g_{cat}h (reproduced with permission from [21] Copyright 2011, Springer).
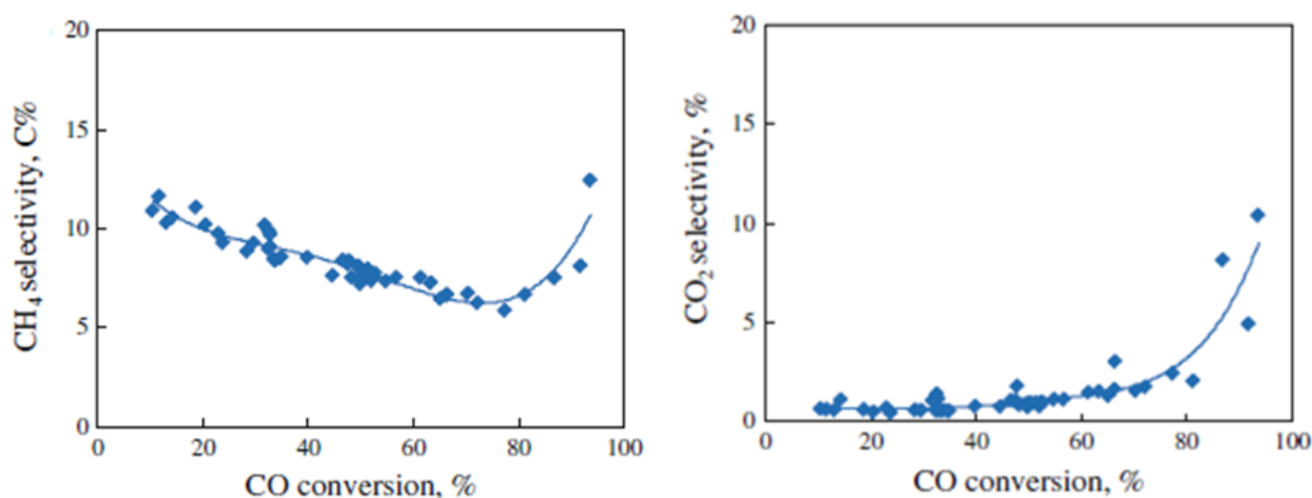
Figure 10. (**left**) Co-feeding of H₂O over 0.5%Pt-15%Co/Al₂O₃ at T = 210 °C, P = 2.0 MPa, H₂:CO = 2:1, SV = 8 SL/g$_{cat}$h reveals that irreversible deactivation (and a minor reversible effect) is observed at 28% H₂O addition; (**right**) XANES analysis of the used catalyst reveals formation of cobalt aluminate through reaction of the CoO formed with the support. Reprinted with permission from [40,49,50]. Copyright (2002, 2003, 2004) Elsevier.
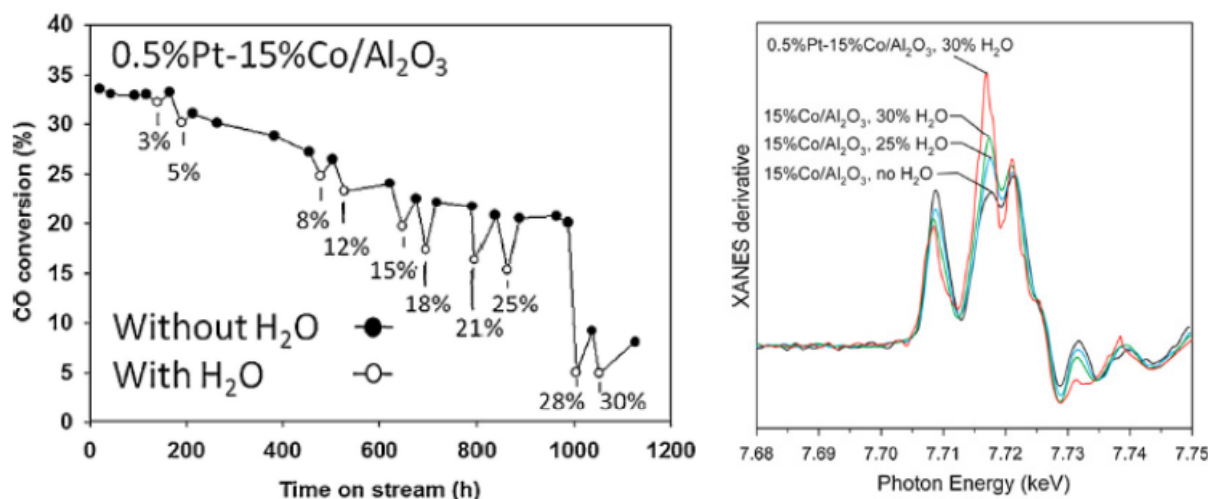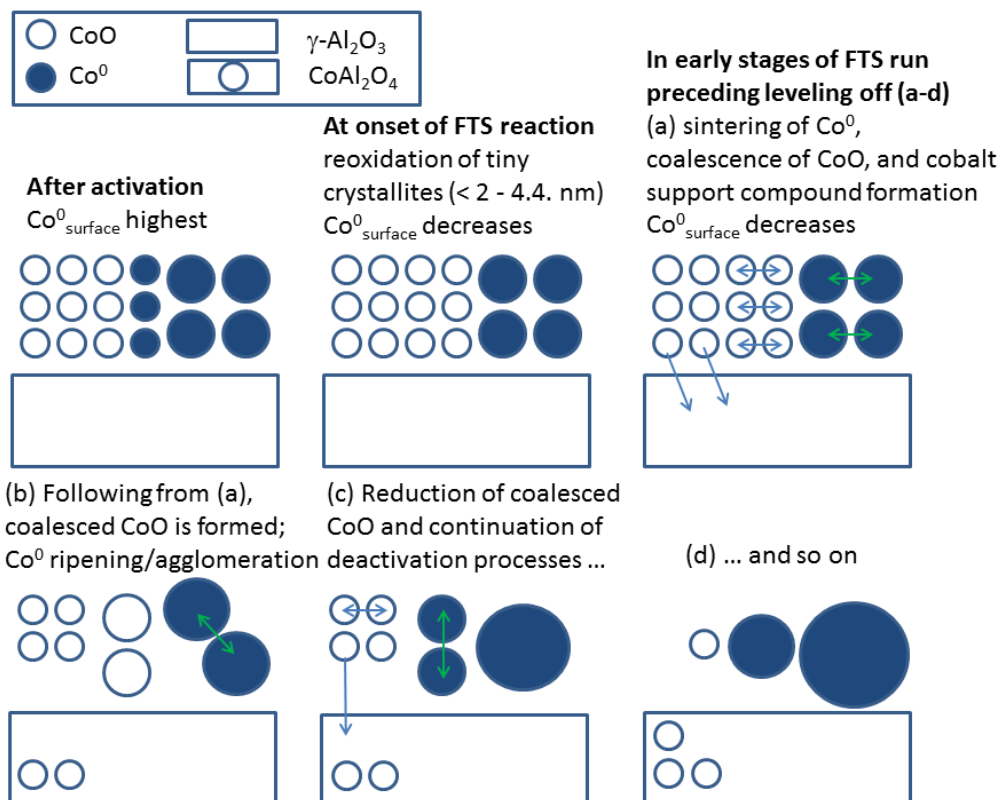

Figure 11. Proposed explanation for the deactivation of alumina-supported cobalt nanoparticles in research catalysts as a function of time on-stream. Adapted with permission from [42]. Copyright (2013) Elsevier [42]. The figure emphasizes why commercial catalysts adopt larger crystallite diameters for the purpose of stability.
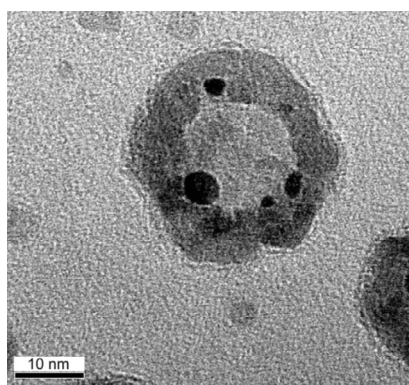
2.3. Regeneration

In recent years, there has been interest in carrying out oxidation-reduction cycles in order to explore the potential for regenerating metal promoted cobalt catalysts. In an earlier work [16], we simulated regeneration with 2%Ru-15%Co/alumina catalysts having relatively high Ru loadings. Part of the aim was to see if any promoter mixing or separation occurred at the atomic level, and the resulting influence on selectivity. To do so, TPR, EXAFS/XANES, and transmission electron microscopy with elemental mapping were applied. It was difficult to detect atomic mixing at the promoter loadings utilized, though elemental mapping showed that the metals were in close proximity to one another at the scale of nanometers. With reduction-oxidation cycles, TPR profiles revealed that while the first step of the TPR shifted to slightly higher temperatures, the second peak (*i.e.*, CoO to Co^0) shifted to slightly lower temperatures [16] for these heavily Ru-loaded catalysts.

Westrate *et al.* [51] compared Pt and Ru promoted Co/alumina catalysts subjected to oxidation-reduction treatments. Following oxidation treatment both the cobalt and promoter phases are well mixed and in an oxidized state. This finding is in agreement with our EXAFS results for a Ag-promoted Co/alumina catalyst [10]. Upon reduction, noble metals form bonds with cobalt metal, again in agreement with our earlier findings for Pt, Re, and Ru promoted catalysts at low promoter loadings [42]. During simulated regeneration by oxidation, the promoter separates from the cobalt phase and is found inside a ring of Co$_3$O$_4$, in "Kirkendall voids" as shown in Figure 12. Re-reduction of this state leads to a decrease in the promoter concentration at the surface of Co particles, as observed by XPS.

Figure 12. Pt promoter (oxide form) is separated from Co$_3$O$_4$ and found within Kirkendall voids within the Co$_3$O$_4$ particle. Reproduced with permission from [51]. Copyright (2013) Elsevier.

A key point regarding regeneration is whether or not the promoter continues to facilitate cobalt oxide reduction once an oxidation (e.g., carbon burn-off) step has been conducted. The proximity of the promoter to cobalt is important; although this will likely vary with promoter chemistry (see earlier comment regarding van Steen's group's use of physical mixtures to demonstrate that atomic contact may not be necessary in all cases [26]). To probe this attribute further, a TPR and XANES investigation was carried out to screen a number of promoter metals [52]. An example comparing two promoters—Pt and Au—is provided in Figure 13 to demonstrate the methodology. The oxidation-reduction cycle involved a 4 h calcination in flowing air at 350 °C followed by reduction for 10 h in hydrogen at

350 °C. It is evident (Figure 13) that Pt improves its effectiveness after three oxidation-reduction cycles, while Au is no longer effective after the first cycle. In the case of Au, the TPR profiles move to higher temperatures with increasing reduction-oxidation cycle number, suggesting that Au is separating from the Co (e.g., by sintering). At the same time, XANES shows that the oxidation state of Co following oxidation reduction moves toward higher oxidation state in the activated Au-promoted catalyst. The TPR profiles for Pt-promoted Co/alumina shift slightly to lower temperature. Corresponding XANES spectra demonstrate that the cobalt is largely reduced after activation following several simulated regeneration cycles. Thus, Pt is a more effective promoter for long-term use, although a different regeneration method at different conditions might be more effective in the case of Au. Both XANES and TPR data revealed that Re retains its ability to facilitate reduction even after 3 oxidation-reduction cycles. With Ru, the XANES results indicated that Ru was also effective after 3 ORcycles, although a slight shift to higher temperature was observed for the CoO to Co^0 TPR peak position in the preliminary study [52].

Figure 13. (**Top**) TPR profiles after RO cycles and (**Bottom**) XANES profiles after RO cycling demonstrate that Pt is more effective at continuing to facilitate reduction after simulate regeneration. Reproduced with permission from [52]. Copyright (2014) Elsevier.
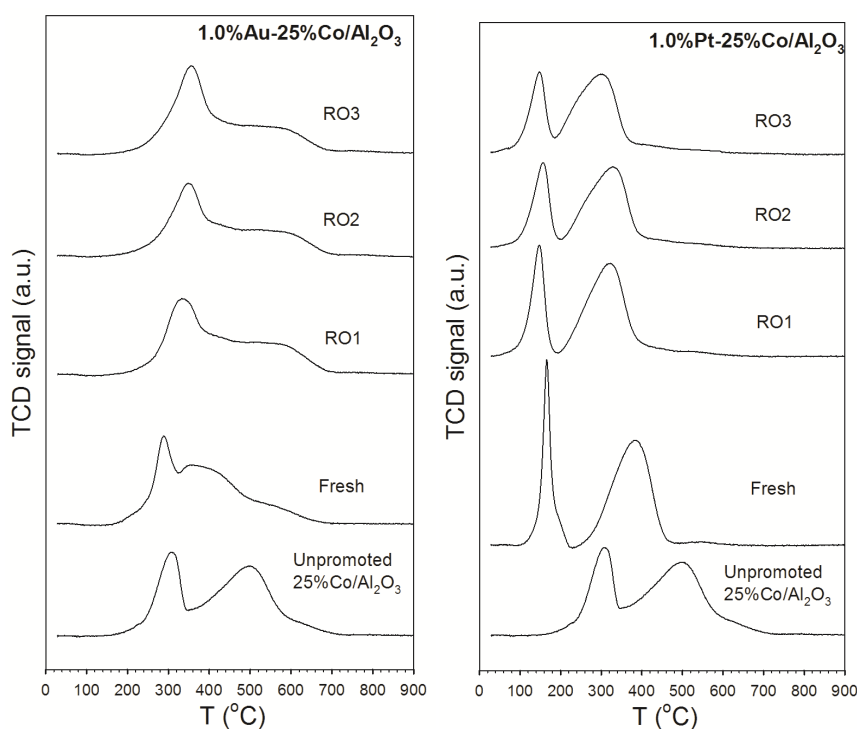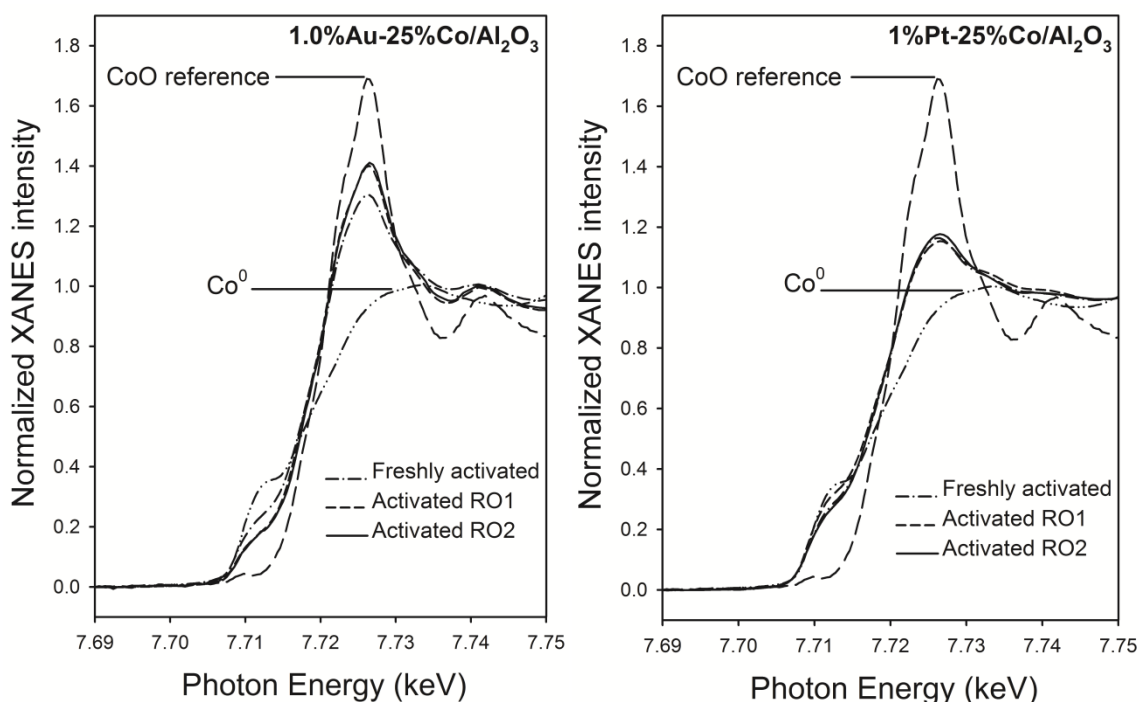
Figure 13. *Cont.*

2.4. Modeling

2.4.1. Modeling of Site Suppression and Deactivation

Although this manuscript is focused on catalyst structure and its influence on FTS stability, a brief word should also be made regarding modeling. One puzzling aspect about the water effect during co-feeding and kinetic investigations is that it can be either positive or negative depending on the nature of the cobalt catalyst. Figure 10 displays results for a 0.5%Pt promoted 15%Co/Al$_2$O$_3$ catalyst having an average cobalt cluster size of 5.6 nm (*i.e.*, crystallites must be equal to below this value), and the water effect is negative but exhibits a significant degree of reversibility at levels below 28 vol.% added H$_2$O. The reversibility was, based on EXAFS/XANES investigations, suggested to be due to oxidation and re-reduction of small cobalt crystallites. Because oxygen was bound to the cobalt sites, the behavior could be modeled in terms of a kinetic parameter based on adsorption inhibition of reactants. On the other hand, Co/silica catalysts having larger cobalt clusters exhibited a positive effect [53], and positive effects on cobalt catalysts have been suggested to be due to water increasing the concentration of surface active carbon species (e.g., unsupported Co and Co/titania [38]) or removing heavy wax from catalyst pores leading to a higher available site density (e.g., Co/silica with varying pore size [54]). Returning to cobalt/alumina catalysts, interestingly, by aging the catalyst sufficiently (*i.e.*, the catalyst is significantly deactivated from its initial condition) [55] or utilizing catalysts with 10+ nm size [56], the deactivation rate becomes low, and the positive kinetic effect occurring on metallic cobalt particles can be observed. The main point is that the water effect can be modeled using a simple power law expression with a water effect parameter, *m*, and the magnitude and sign (*i.e.*, positive [57] or negative [55,57]) of *m* provides valuable information about the structure of the catalyst.

$$r(FT) = kP(CO)^a P(H_2)^b / [1 + m\, P(H_2O)/P(H_2)] \tag{1}$$

A number of the phenomena associated with the stability and deactivation of cobalt catalysts have been discussed herein, and these and other aspects of stability (e.g., carbon deposition and carbide formation) are discussed in the Editor's book on Catalyst Deactivation [58] and a review article [59]. At this point in time, a number of important aspects and trends regarding the structure sensitivity of cobalt catalysts, and especially experimental research catalysts, are known. However, moving forward, there is a great deal of focus on developing catalysts that make the most efficient use of cobalt. Co crystallites should be small enough to maximize active site density, but also large enough that crystallites will be stabilized against reoxidation and sintering. Researchers are also exploring preparation methods to disperse and adequately position metal clusters in spatially favorable ways (*i.e.*, as far apart as possible). Some methods include freeze-drying [60], vapor phase impregnation [61], coating the support with carbon [62], using solvents such as ethylene glycol [63], optimizing drying temperature or calcination chemistry with dilute NO/N_2 [64], bypassing calcination altogether [53], or locking metal particles onto the support so that they cannot find one another and undergo agglomeration [65]. Thus, using advanced preparation methods to obtain spatially uniform distribution of cobalt crystallites is critical, since in conventional cobalt/alumina catalysts prepared by impregnation, cobalt clusters can be within close vicinity to one another, or in grapelike clusters, which have been described as "graveyards" for cobalt active sites during reaction testing [66]. Thus, thinking toward the future, it will be of increasing importance to model deactivation mechanisms and quantify how much each mechanism contributes to overall deactivation of the catalyst. Robust models which address the chemistry of promoters could enable the performance of new research catalysts to be compared to current commercial catalyst formulations. For example, a recently published forward thinking article by Argyle *et al.* [67] addresses modeling of the contributions of several deactivation mechanisms to overall deactivation rate in Co catalyzed FTS.

2.4.2. Computational Methods Based on First Principles

Related to promoters of FTS catalysts, computational methods based on first principles have been useful in describing the location of promoter with respect to cobalt, for providing insight into the requirements for cobalt oxidation by H_2O, and for determining how the promoter may influence carbon deposition.

Computational methods are being utilized to elucidate the preferential location for the occupancy of the promoter with respect to the cobalt atoms that make up the cluster. For example, a combined study making using of Low Energy Ion Scattering (*i.e.*, on a 1%Re-12%Co/Al$_2$O$_3$ catalyst) and computational DFT modeling (*i.e.*, on a Co$_{13}$Re cluster) determined that there is a preference of Re promoter to occupy subsurface sites, where it coordinates with a maximum number of cobalt atoms [68]. This is in agreement with the results of some EXAFS investigations, where direct Re-Co atomic contact has been observed [19,20].

Molecular modeling has also been conducted to examine surface oxidation of larger cobalt particles (e.g., as utilized in commercial catalysts) by H_2O, and the pathway was ruled out as a significant chemical transformation mechanism for deactivating sites under commercial FTS conditions [31].

Computational methods have also been used extensively to gain insight into the role of carbon deposits in catalyst deactivation. For example [69], HR-TEM and computational DFT modeling were applied to elucidate the preferred occupancies of carbon over different cobalt surfaces. The stability of various carbon species under reaction conditions was evaluated. Extended graphene islands and a surface carbide were found to be 99 and 79 kJ/mol more stable than surface CH_2 groups. Both carbon phases were suggested to initiate and grow from step sites. Saib *et al.* [31] have recently reviewed carbon formation in detail on cobalt FTS catalysts, including the application of computational methods. They also analyzed used catalysts from a commercial slurry bubble column reactor and, following wax extraction by THF, carried out temperature programmed hydrogenation and oxidation measurements to characterize the carbons. The least reactive species toward hydrogenation, which reacted at 430 °C, was assigned to polymeric carbons. A model [70] showing the location of small carbon oligomers of the fcc Co(111) surface, the precursors of polymeric carbon, was described. Note that polymeric carbon was found on both cobalt and the support. The authors [31] also reviewed the role of subsurface carbon [69,71], where theoretical modeling has indicated that subsurface carbon hinders CO adsorption and dissociation processes on associated Co atoms, and the requirements under which carbon induces clock surface reconstruction [72]. This, in turn, may cause deactivation of sites via shape changes or, on the other hand, induce the formation of active sites (e.g., B5 sites [31]: 3-fold sites that more easily dissociate CO; or triangular nanoscale islands having step edges similar to C7 sites [73], as observed by scanning tunneling microscopy). The restructuring of cobalt by strong CO chemisorption (*i.e.*, roughening—leading to more active sites) was described by Schulz *et al.* [74] as to be in competition with sintering.

Some computational studies have focused on defining how promoters of cobalt catalysts may impact carbon formation. Recently, the mechanisms for carbon compound formation on unpromoted and Pt or Ru promoted Co surfaces were investigated [75]. The activation energies for carbon-carbon and carbon-carbon-carbon coupling reactions were found to be larger on Pt or Ru promoted Co surfaces relative to unpromoted Co surface. The results suggest that carbon formation and thus, carbon compound (e.g., polymeric carbon formation, may be inhibited by the presence of the promoters. The authors also found that the promoters did not change the activation energy of C diffusion to the subsurface.

3. Experimental Section

Typical catalyst preparation method: the support used was Sasol Catalox-150 γ-Al_2O_3. It was first calcined at 400 °C in a muffle furnace for 4 h. A slurry impregnation method was performed, whereby the ratio of the volume of loading solution used to the weight of alumina was 1:1, such that approximately 2.5 times the pore volume of solution was used to prepare the catalyst in two steps [7]. Due to the solubility limit of cobalt nitrate, multiple impregnation steps were used. After each impregnation step, the catalyst was dried under vacuum in a rotary evaporator from 80 to 100 °C. Promoter precursors used were tetraammine palladium (II) nitrate, tetraammine platinum (II) nitrate, rhenium oxide (Re_2O_7), ruthenium nitrosyl nitrate, silver nitrate, $HAuCl_4$, and copper nitrate. The promoters were added dropwise to achieve incipient wetness impregnation. After final drying at 80–100 °C, the final catalysts were calcined at 350 °C under flowing air for 4 h.

Typical CSTR reaction test: the catalyst (15 g) was ground and sieved to 170–325 mesh before loading into a fixed-bed reactor for 10–15 h of ex situ reduction at 350 °C and atmospheric pressure using a gas mixture of H_2/He with a molar ratio of 1:3. The reduced catalyst was then transferred to a 1-L continuously stirred tank reactor (CSTR) which was previously charged with 315 g of melted Polywax 3000, under the protection of a N_2 inert gas. The transferred catalyst was further reduced *in situ* at 230 °C at atmospheric pressure using pure hydrogen for another 10 h before starting the FT reaction. In this study, the FT conditions were 220 °C, 1.5–2.2 MPa, H_2/CO = 2.0–2.1. The space velocity varied between 1.0 and 16 NL/g-cat/h. in order to give about 50% CO conversion in different tests. This allowed us to fairly compare the differences in hydrocarbon selectivity data resulting from the promoter effect.

4. Conclusions

There are a number of stability issues that must be considered when selecting metal reduction promoters for use in Fischer-Tropsch synthesis catalysts. If tiny cobalt crystallites (<2–4.4 nm) are formed by facilitating the reduction of cobalt oxides that are strongly interacting with the support, they may undergo reoxidation at the onset of FTS at high conversion. Any cobalt oxide either left unreduced or formed from reoxidation of tiny cobalt crystallites can participate in a complex sintering mechanism that involves agglomeration of cobalt oxides, re-reduction, and sintering of the metal. Promoters can also exacerbate sintering if the cobalt metal clusters formed as a result of the promoting effect are in close proximity to other cobalt particles on the surface. Not all metals that facilitate cobalt reduction promote activity on a per gram catalyst basis; some will poison the surface (e.g., Cu). A poor choice of promoter (or poor choice in loading) can also lead to excessive hydrogenation activity and raise the light gas selectivity (e.g., Pd or Cu; Au at high loading). Furthermore, certain metals (e.g., Au) that promote cobalt oxide reduction can separate from cobalt during oxidation-reduction (regeneration) cycles. Therefore, they may not be effective for long-term use, or they may require non-standard regeneration treatments. Computational studies suggest that certain promoters (e.g., Pt or Ru) may hinder deactivation by carbon by increasing the energy barrier for carbon-carbon coupling reactions, while subsurface C formation was not found to be affected.

Acknowledgments

Conflicts of Interest

The authors declare no conflict of interest.

References

1. Espinoza, R.L.; Visagie, J.L.; van Berge, P.J.; Bolder, F.H. Fischer-Tropsch catalysts containing iron and cobalt. US Patent No. 5,733,839, March 1998.

2. Van Berge, P.J.; Barradas, S.; van de Loosdrecht, J.; Visagie, J.L. Advances in the cobalt catalyzed Fischer-Tropsch synthesis. *Erdöl Erdgas Kohle* **2001**, *117*, 138–142.

3. Wang, W.-J.; Chen, Y.-W. Influence of metal loading on the reducibility and hydrogenation activity of cobalt/alumina catalysts. *Appl. Catal.* **1991**, *77*, 223–233.

4. Jacobs, G.; Ji, Y.; Davis, B.H.; Cronauer, D.C.; Kropf, A.J.; Marshall, C.L. Fischer-Tropsch synthesis: Temperature programmed EXAFS/XANES investigation of the influence of support type, cobalt loading, and noble metal promoter addition to the reduction behavior of cobalt oxide particles. *Appl. Catal. A* **2007**, *333*, 177–191.

5. Reuel, R.C.; Bartholomew, C.H. The stoichiometries of H_2 and CO adsorptions on cobalt: Effects of support and preparation. *J. Catal.* **1984**, *85*, 63–77.

6. Vada, S.; Hoff, A.; Adnanes, E.; Schanke, D.; Holmen, A. Fischer-Tropsch synthesis on supported cobalt catalysts promoted by platinum and rhenium. *Top. Catal.* **1995**, *2*, 155–162.

7. Jacobs, G.; Das, T.K.; Zhang, Y.-Q.; Li, J.; Racoillet, G.; Davis, B.H. Fischer-Tropsch synthesis: support, loading, and promoter effects on the reducibility of cobalt catalysts. *Appl. Catal. A* **2002**, *233*, 263–281.

8. Farrauto, R.J.; Bartholomew, C.H. *Fundamentals of Industrial Catalytic Processes*; John Wiley & Sons: Chichester, UK, 2003; p. 700.

9. Cook, K.M.; Poudyal, S.; Miller, J.T.; Bartholomew, C.H.; Hecker, W.C. Reducibility of alumina-supported cobalt Fischer-Tropsch catalysts: Effects of noble metal type, distribution, retention, chemical state, bonding, and influence on cobalt crystallite size. *Appl. Catal. A* **2012**, *449*, 69–80.

10. Jacobs, G.; Ribeiro, M.C.; Ma, W.; Ji, Y.; Khalid, S.; Sumodjo, P.T.A.; Davis, B.H. Group 11 (Cu, Ag, Au) promotion of 15%Co/Al_2O_3 Fischer-Tropsch synthesis catalysts. *Appl. Catal. A* **2009**, *361*, 137–151.

11. Aldossary, M.A.; Sharma, P.; Ojeda, M.; Gupta, M.; Fierro, J.L.; Spivey, J.J. Effect of different Cu loading on Fe-Mg catalyst for Fischer-Tropsch synthesis. In Proceedings of ACS National Meeting & Exposition, Philadelphia, PA, USA, August 19–23, 2012. Curran Associates, Inc.: Red Hook, NY, USA, 2012; Volume 57, p. 944.

12. Li, S.; Li, A.; Krishnamoorthy, S.; Iglesia, E. Effects of Zn, Cu, and K promoters on the structure and on the reduction, carburization, and catalytic behavior of iron-based Fischer-Tropsch synthesis catalysts. *Catal. Lett.* **2001**, *77*, 197–205.

13. Cesar, D.V.; Perez, C.A. Quantitative XPS analysis of bimetallic Cu-Co catalysts. *Phys. Status Solidi A* **2001**, *187*, 321–326.

14. Todic, B.; Bhatelia, T.; Froment, G.F.; Ma, W.; Jacobs, G.; Davis, B.H.; Bukur, D.B. Kinetic model of Fischer-Tropsch synthesis in a slurry reactor on Co/Re/Al_2O_3 catalyst. *Ind. Eng. Chem. Res.* **2013**, *52*, 669–679.

15. Jacobs, G.; Ma, W.; Gao, P.; Todic, B.; Bhatelia, T.; Bukur, D.B.; Khalid, S.; Davis, B.H. Fischer-Tropsch synthesis: differences observed in local atomic structure and selectivity with Pd compared to typical promoters (Pt, Re, Ru) of Co/Al_2O_3 catalysts. (Special Issue in honor of the late Prof. Laszlo Guczi 1932–2012). *Top. Catal.* **2012**, *55*, 811–817.

16. Jacobs, G.; Sarkar, A.; Ji, Y.; Luo, M.-S.; Dozier, A.; Davis, B.H. Fischer-Tropsch synthesis: assessment of the ripening of cobalt clusters and mixing between Co and Ru promoter via oxidation-reduction cycles over lower Co-loaded Ru-Co/Al$_2$O$_3$ catalysts. *Ind. Eng. Chem. Res.* **2008**, *47*, 672–680.

17. Borg, O.; Hammer, N.; Eri, S.; Lindvag, O.A.; Myrstad, R.; Blekkan, E.A.; Ronning, M.; Rytter, E.; Holmen, A. Fischer-Tropsch synthesis over un-promoted and Re-promoted gamma-Al$_2$O$_3$ supported cobalt catalysts with different pore sizes. *Catal. Today* **2009**, *142*, 70–77.

18. Bazin, D.; Borko, L.; Koppany, Zs.; Kovacs, I.; Stefler, G.; Sajo, L.I.; Schay, Z.; Guczi, L. Re-Co/NaY and Re-Co/Al$_2$O$_3$ bimetallic catalysts: *In situ* EXAFS and catalytic activity. *Catal. Lett.* **2002**, *84*, 169–182.

19. Jacobs, G.; Chaney, J.A.; Patterson, P.M.; Das, T.K.; Davis, B.H. Fischer-Tropsch synthesis: Study of the promotion of Re on the reduction property of Co/Al$_2$O$_3$ catalysts by *in situ* EXAFS/XANES of Co K and Re L$_{III}$ edges and XPS. *Appl. Catal. A* **2004**, *264*, 203–212.

20. Ronning, M.; Nicholson, D.G.; Holmen, A. *In situ* EXAFS study of the bimetallic interaction in a rhenium-promoted alumina-supported cobalt Fischer-Tropsch catalyst. *Catal. Lett.* **2001**, *72*, 141–146.

21. Ma, W.; Jacobs, G.; Ji, Y.; Bhatelia, T.; Bukur, D.B.; Khalid, S.; Davis, B.H. Fischer-Tropsch synthesis: Influence of CO conversion on selectivities, H$_2$/CO usage ratios, and catalyst stability for a Ru promoted Co/Al$_2$O$_3$ catalyst using a slurry phase reactor. *Top. Catal.* **2011**, *54*, 757–767.

22. Guczi, L.; Bazin, D.; Kovacs, I.; Borko, L.; Schay, Z.; Lynch, J.; Parent, P.; Lafon, C.; Stefler, G.; Koppany, Z.; Sajo, I. Structure of Pt-Co/Al$_2$O$_3$ and Pt-Co/NaY bimetallic catalysts: Characterization by *in situ* EXAFS, TPR, XPS and by activity in CO (Carbon Monoxide) Hydrogenation. *Top. Catal.* **2002**, *20*, 129–139.

23. Jacobs, G.; Chaney, J.A.; Patterson, P.M.; Das, T.K.; Maillot, J.C.; Davis, B.H. Fischer-Tropsch synthesis: Study of the promotion of Pt on the reduction property of Co/Al$_2$O$_3$ catalysts by *in situ* EXAFS of Co K and Pt L$_{III}$ edges and XPS. *J. Synch. Rad.* **2004**, *11*, 414–422.

24. Sadeqzadeh, M.; Karaca, H.; Safonova, O.V.; Fongarland, P.; Chambrey, S.; Roussel, P.; Griboval-Constant, A.; Lacroix, M.; Curulla-Ferré, D.; Luck, F.; *et al.* Identification of the active species in the working alumina-supported cobalt catalyst under various conditions of Fischer–Tropsch synthesis. *Catal. Today* **2011**, *164*, 62–67.

25. Iglesia, E.; Soled, S.L.; Fiato, R.A.; Via, G.H. Bimetallic synergy in cobalt-ruthenium Fischer-Tropsch synthesis catalysts. *J. Catal.* **1993**, *143*, 345–368.

26. Chonco, Z.H.; Nabaho, D.; Claeys, M.; van Steen, E. The role of reduction promoters in Fischer-Tropsch catalysts for the production of liquid fuels. In Proceedings of 23rd Meeting of the North American Catalysis Society, 2–7 June 2013, Louisville, KY, USA.

27. Ionkina, O.; Subramanian, M.A.; Chao, W.; Makar, K.M.; Manzer, L.E. Fischer-Tropsch processes and catalysts with promoters. *US Patent* 20020010221A1, January 2002.

28. Jermwongratanachai, T.; Jacobs, G.; Ma, W.; Shafer, W.D.; Gnanamani, M.K.; Gao, P.; Kitiyanan, B.; Davis, B.H.; Klettlinger, J.L.S.; Yen, C.H.; *et al.* Fischer-Tropsch synthesis: Comparisons between Pt and Ag promoted Co/Al$_2$O$_3$ catalysts for reducibility, local atomic structure, catalytic activity, and oxidation-reduction (OR) cycles. *Appl. Catal.* **2013**, *464–465*, 165–180.

29. Redjala, T.; Remita, H.; Apostolescu, G.; Mostafavi, M.; Thomazeau, C.; Uzio, D. Bimetallic Au-Pd and Ag-Pd clusters synthesized by gamma or electron beam radiolysis and study of the reactivity/structure relationships in the selective hydrogenation of but-1,3-diene. *Oil Gas Sci. Technol.* **2006**, *61*, 789–797.

30. Van Steen, E.; Claeys, M.; Dry, M.E.; van de Loosdrecht, J.; Viljoen, E.L.; Visagie, J.L. Stability of nanocrystals: thermodynamic analysis of oxidation and re-reduction of cobalt in water/hydrogen mixtures. *J. Phys. Chem. B* **2005**, *109*, 3575–3577.

31. Saib, A.M.; Moodley, D.J.; Ciobica, I.M.; Hauman, M.M.; Sigwebela, B.H.; Weststrate, C.J.; Niemantsverdriet, J.W.; van de Loosdrecht, J. Fundamental understanding of deactivation and regeneration of cobalt Fischer-Tropsch synthesis catalysts. *Catal. Today* **2010**, *154*, 271–282.

32. Saib, A.M.; Borgna, A.; van de Loosdrecht, J.; van Berge, P.J.; Niemantsverdriet, J.W. XANES study of the susceptibility of nano-sized cobalt crystallites to oxidation during realistic Fischer-Tropsch synthesis. *Appl. Catal.* **2006**, *312*, 12–19.

33. Bezemer G.L, Bitter J.H.; Kuipers H.P.C.E.; Oosterbeek H.; Holewijn J.E.; Xu X.D.; Kapteijn, F.; van Dillen, A.J.; de Jong, K.P. Cobalt particle size effects in the Fischer-Tropsch reaction studied with carbon nanofiber supported catalysts. *J. Am. Chem. Soc.* **2006**, *128*, 3956–3964.

34. Borg, Ø.; Dietzel, P.D.C.; Spjelkavik, A.I.; Tveten, E.Z.; Walmsley, J.C.; Diplas, S.; Eri, S.; Holmen, A.; Rytter, E. Fischer-Tropsch synthesis: cobalt particle size and support effects on intrinsic activity and product distribution. *J. Catal.* **2008**, *259*, 161–164.

35. Azzam, K.; Jacobs, G.; Ma, W.; Davis, B.H. Effect of cobalt particle size on the catalyst intrinsic activity for Fischer-Tropsch synthesis. *Catal. Lett.* **2014**, *144*, 389–394.

36. Jermwongratanachai, T.; Jacobs, G.; Shafer, W.D.; Ma, W.; Pendyala, V.R.R.; Davis, B.H.; Kitiyanan, B.; Khalid, S.; Cronauer, D.C.; Kropf, A.J.; Marshall, C.L. Fischer-Tropsch synthesis: Oxidation of a fraction of cobalt crystallites in research catalysts at the onset of FT at partial pressures mimicking 50% CO conversion. *Top. Catal.* in press.

37. Fischer, N.; Clapham, B.; Feltes, T.E.; van Steen, E.; Claeys, M. The reoxidation of cobalt Fischer-Tropsch catalysts. In Proceedings of Syngas 2012 Convention, Cape Town, South Africa, 1–4 April 2012.

38. Bertole, C.J.; Mims, C.A.; Kiss, G. The effect of water on the cobalt-catalyzed Fischer-Tropsch synthesis. *J. Catal.* **2002**, *210*, 84–96.

39. Sadeqzadeh, M.; Hong, J.; Fongarland, P.; Curulla-Ferre, D.; Luck, F.; Bousquet, J.; Schweich, D.; Khodakov, A.Y. Mechanistic modeling of cobalt based catalyst sintering in a fixed bed reactor under different conditions of Fischer-Tropsch synthesis. *Ind. Eng. Chem. Res.* **2012**, *51*, 11955–11964.

40. Jacobs, G.; Das, T.K.; Patterson, P.M.; Luo, M.; Conner, W.A.; Davis, B.H. Fischer-Tropsch synthesis: Effect of water on Co/Al$_2$O$_3$ catalysts and XAFS characterization of reoxidation phenomena. *Appl. Catal. A* **2004**, *270*, 65–76.

41. Soled, S.; Kliewer, C.; Kiss, G.; Baumgartner, J. Reversible and irreversible changes in Co Fischer-Tropsch catalysts during synthesis. In Proceedings of 21st Meeting of the North American Catalysis Society, San Francisco, CA, USA, 7–12 June 2009.

42. Jacobs, G.; Ma, W.; Gao, P.; Todic, B.; Bhatelia, T.; Bukur, D.B.; Davis, B.H. The application of synchrotron methods in characterizing iron and cobalt Fischer-Tropsch synthesis catalysts. *Catal. Today* **2013**, *214*, 100–139.

43. Moodley, D.J.; Saib, A.M.; van de Loosdrecht, J.; Welker-Nieuwoudt, C.A.; Sigwebela, B.H.; Niemantsverdriet, J.W. The impact of cobalt aluminate formation on the deactivation of cobalt-based Fischer-Tropsch synthesis catalysts. *Catal. Today* **2011**, *171*, 192–200.

44. Das, T.K.; Jacobs, G.; Patterson, P.M.; Conner, W.A.; Davis, B.H. Fischer-Tropsch synthesis: Characterization and catalytic properties of rhenium promoted cobalt alumina catalysts. *Fuel* **2003**, *82*, 805–815.

45. Jacobs, G.; Sarkar, A.; Ji, Y.; Patterson, P.M.; Das, T.K.; Luo, M.; Davis, B.H. Fischer-Tropsch synthesis: characterization of interactions between reduction promoters and Co for Co/Al_2O_3–based GTL catalysts. In Proceedings of *AIChE Annual Meeting*, San Francisco, CA, USA, 12–17 November 2006.

46. Karaca, H.; Hong, J.; Fongarland, P.; Roussel, P.; Griboval-Constant, A.; Lacroix, M.; Hortmann, K.; Safonova, O.V.; Khodakov, A.Y. *In situ* XRD investigation of the evolution of alumina-supported cobalt catalysts under realistic conditions of Fischer-Tropsch synthesis. *Chem. Commun.* **2010**, *46*, 788–790.

47. Jacobs, G.; Patterson, P.M.; Zhang, Y.-Q.; Das, T.K.; Li, J.; Davis, B.H. Fischer-Tropsch synthesis: Deactivation of noble metal-promoted Co/Al_2O_3 catalysts. *Appl. Catal. A* **2002**, *233*, 215–226.

48. Kim, C.J. Water addition for increased CO/H_2 hydrocarbon activity over catalysts comprising * e There is virtually no difference. carried out for thousands of hours, the time ranges specified are very close to each othecobalt, ruthenium, and mixtures thereof which may include a promoter metal. U.S. Patent 5,227,407, July 1993.

49. Li, J.; Zhan, X.; Zhang, Y.-Q.; Jacobs, G.; Das, T.K.; Davis, B.H. Fischer-Tropsch synthesis: Effect of water on the deactivation of Pt promoted Co/Al_2O_3 catalysts. *Appl. Catal. A* **2002**, *228*, 203–212.

50. Jacobs, G.; Das, T.K.; Patterson, P.M.; Li, J.; Sanchez, L.; Davis, B.H. Fischer-Tropsch synthesis: XAFS studies of the effect of water on a Pt-promoted Co/Al_2O_3 catalyst. *Appl. Catal. A* **2003**, *247*, 335–343.

51. Weststrate, C.J.; Saib, A.M.; Niemantsverdriet, J.W. Promoter segregation in Pt and Ru promoted cobalt model catalysts during oxidation-reduction treatments. *Catal. Today* **2013**, *215*, 2–7.

52. Jermwongratanachai, T.; Jacobs, G.; Shafer, W.D.; Pendyala, V.R.R.; Ma, W.; Gnanamani, M.K.; Hopps, S.; Thomas, G.A.; Kitiyanan, B.; Khalid, S.; *et al.* Fischer-Tropsch synthesis: TPR and XANES analysis of the impact of oxidation-reduction (OR) cycles on the reducibility of Co/alumina catalysts with different promoters (Pt, Ru, Re, Ag, Au, Rh, Ir). *Catal. Today* 2014, in press.

53. Li, J.; Jacobs, G.; Das, T.K.; Zhang, Y.-Q.; Davis, B.H. Fischer-Tropsch synthesis: Effect of water on the catalytic properties of a Co/SiO$_2$ catalyst. *Appl. Catal. A* **2002**, *236*, 67–76.

54. Dalai, A.K.; Das, T.K.; Chaudhari, K.V.; Jacobs, G.; and Davis, B.H. Fischer-Tropsch synthesis: Water effects on Co supported on wide and narrow-pore silica. *Appl. Catal. A* **2005**, *289*, 135–142.

55. Ma, W.; Jacobs, G.; Sparks, D.E.; Spicer, R.L.; Davis, B.H.; Klettlinger, J.L.S.; Yen, C.H. Fischer-Tropsch synthesis: Kinetics and water effect study over 25%Co/Al$_2$O$_3$ catalysts. *Catal. Today* **2014**, in press.

56. Logdberg, S.; Boutonnet, M.; Walmsley, J.C.; Jaras, S.; Holmen, A.; Blekkan, E.A. Effect of water on the space-time yield of different supported cobalt catalysts during Fischer-Tropsch synthesis. *Appl. Catal. A* **2011**, *393*, 109–121.

57. Ma, W.; Jacobs, G.; Sparks, D.E.; Gnanamani, M.K.; Pendyala, V.R.R.; Yen, C.H.; Klettlinger, J.L.S.; Tomsik, T.M.; Davis, B.H. Fischer-Tropsch synthesis: support and cobalt cluster size effects on kinetics over Co/Al$_2$O$_3$ and Co/SiO$_2$ catalysts. *Fuel* **2011**, *90*, 756–765.

58. Studies in Surface Science and Catalysis. *Catalyst Deactivation 1991: Proceedings of the 5th International Symposium*; Bartholomew, C.H., Butt, J.B., Eds.; Elsevier: Amsterdam, The Netherlands, 1991; Volume 68.

59. Bartholomew, C.H. Mechanisms of catalyst deactivation. *Appl. Catal. A* **2001**, *212*, 17–60.

60. Eggenhuisen, T.M.; Munnik, P.; Talsma, H.; de Jongh, P.E.; de Jong, K.P. Freeze-drying for controlled nanoparticle distribution in Co/SiO$_2$ Fischer-Tropsch catalyst. *J. Catal.* **2013**, *297*, 306–313.

61. Graham, U.M.; Jacobs, G.; Gnanamani, M.; Lipka, S.; Shafer, W.D.; Swartz, C.; Jermwongratanachai, T.; Chen, R.; Rogers, F.; Davis, B.H. Fischer Tropsch Synthesis: High Oxygenate-Selectivity of Cobalt Catalysts supported on Hydrothermal Carbons. *ACS Catal.* submitted for publication, 2014.

62. van de Loosdrecht, J.; Datt, M.; Visagie, J.L. Carbon coated supports for cobalt based Fischer-Tropsch catalysts. *Top. Catal.* 2014, in press.

63. Rane, S.; Borg, O.; Yang, J.; Rytter, E.; Holmen, A. Effect of alumina phases on hydrocarbon selectivity in Fischer-Tropsch synthesis. *Appl. Catal. A* **2010**, *388*, 160–167.

64. Sietsma, J.R.A.; den Breejen, J.P.; de Jongh, P.E.; van Dillen, J.; Bitter, J.H.; de Jong, K.P. Highly active cobalt-on-silica catalysts for the Fischer-Tropsch synthesis obtained via a novel calcination. *Stud. Surf. Sci. Catal.* **2007**, *167*, 85–90.

65. Lu, J.; Elam, J.W.; Stair, P.C. Synthesis and stabilization of supported metal catalysts by atomic layer deposition. *Accts. Chem. Res.* **2013**, *46*, 1806–1815.

66. Soled, S.L.; Kiss, G.; Kliewer, C.; Baumgartner, J.; El-Malki, E.-M. Learnings from Co Fischer-Tropsch catalyst studies. Abstracts of Papers, ENFL-412, 245th ACS National Meeting & Exposition, New Orleans, LA, USA, 7–11 April 2013.

67. Argyle, M.D.; Frost, T.S.; Bartholomew, C.H. Cobalt Fischer Tropsch catalyst deactivation modeled using generalized power law expressions. *Top. Catal.* 2014, in press.

68. Bakken, V.; Bergene, E.; Rytter, E.; Swang, O. Bimetallic cobalt/rhenium systems: Preferred position of rhenium through an interdisciplinary approach. *Catal. Lett.* **2010**, *135*, 21–25.

69. Tan, K.F.; Xu, J.; Chang, J.; Borgna, A.; Saeys, M. Carbon deposition on Co catalysts during Fischer-Tropsch synthesis: A computational and experimental study. *J. Catal.* **2010**, *274*, 121–129.

70. Swart, J.C.W.; Ciobica, I.M.; van Santen, R.A.; van Steen, E. Intermediates in the formation of graphitic carbon on a flat FCC-Co(111) surface. *J. Phys. Chem. C* **2008**, *112*, 12899–12904.

71. Burghgraef, H. A quantum chemical study of CH and CC bond activation on transition metals. PhD Thesis, Eindhoven University of Technology: Eindhoven, The Netherlands, June 1995.

72. Ciobica, I.M.; van Santen, R.A.; van Berge, P.J.;. van de Loosdrecht, J. Adsorbate induced reconstruction of cobalt surfaces. *Surf. Sci.* **2008**, *602*, 17–27.

73. Wilson, J.; de Groot, C. Atomic-scale restructuring in high-pressure catalysis. *J. Phys. Chem.* **1995**, *99*, 7860–7866.

74. Schulz, H.; Nie, Z.; Ousmanov, F. Construction of the Fischer–Tropsch regime with cobalt catalysts. *Catal. Today* **2001**, *71*, 351–360.

75. Balakrishnan, N.; Joseph, B.; Bhethanabotla, V.R. Effect of Pt and Ru promoters on deactivation of Co catalysts by C deposition during Fischer-Tropsch synthesis: A DFT study. *Appl. Catal. A* **2013**, *462–463*, 107–115.